Damping in yttrium iron garnet films with interface

Ravinder Kumar,[1,2,*] B. Samantaray,[1] Shubhankar Das,[3] Kishori Lal,[1] D. Samal,[2,4] and Z. Hossain[1,5,†]

[1]*Department of Physics, Indian Institute of Technology, Kanpur 208016, India*

[2]*Institute of Physics, Bhubaneswar 751005, India*

[3]*Institute of Physics, Johannes Gutenberg University Mainz, 55099 Mainz, Germany*

[4]*Homi Bhabha National Institute, Anushakti Nagar, Mumbai 400085, India*

[5]*Institute of Low Temperature and Structure Research, 50-422 Wroclaw, Poland*

(Received 17 August 2021; revised 18 June 2022; accepted 19 July 2022; published 2 August 2022)

We report strong damping enhancement in yttrium iron garnet (YIG) film due to spin inhomogeneity at the interface. The growth-induced thin interfacial gadolinium iron garnet (GdIG) layer antiferromagnetically (AFM) exchange couples with the top YIG layer. The out-of-plane angular variation of ferromagnetic resonance linewidth ΔH reflects a large inhomogeneous distribution of the effective magnetization $\Delta 4\pi M_{\rm eff}$ due to the presence of the aforementioned AFM exchange coupling between the interfacial-GdIG and top-YIG layer. We probe the spin inhomogeneity at the YIG-GdIG interface by performing an in-plane angular variation of resonance field H_r, leading to a unidirectional feature. The large extrinsic $\Delta 4\pi M_{\rm eff}$ contribution, apart from the inherent intrinsic Gilbert contribution, manifests enhanced precessional damping in the YIG film.

DOI: 10.1103/PhysRevB.106.054405

I. INTRODUCTION

The viability of spintronics demands novel magnetic materials and $Y_3Fe_5O_{12}$ (YIG) is a potential candidate as it exhibits ultralow precessional damping, $\alpha \sim 3 \times 10^{-5}$ [1]. The magnetic properties of YIG thin films epitaxially grown on top of $Gd_3Ga_5O_{12}$ (GGG) vary significantly due to growth tuning [2,3], film thickness [4], heavy-metal substitution [5–7], and coupling with thin metallic layers [8–10]. The growth processes may also induce the formation of a thin interfacial $Gd_3Fe_5O_{12}$ (GdIG) layer at the YIG-GGG interface [11–13]. The YIG-GdIG heterostructure derived out of monolithic YIG film growth on GGG exhibits interesting phenomena such as an all-insulating equivalent of a synthetic antiferromagnet [12] and hysteresis loop inversion governed by positive exchange bias [13]. The YIG-GdIG heterostructure are of great interest as these can be further exploited for the optimization of different functionalities in insulating spintronic devices. The writing and reading operations with spin-orbit torque and spin Hall magnetoresistance, respectively, are also a possibility in insulating magnetic memories [12].

The relaxation of magnetic excitation toward equilibrium is governed by intrinsic and extrinsic mechanisms, leading to a finite ferromagnetic resonance linewidth (ΔH) [14,15]. The former mechanism dictates Gilbert-type relaxation, a consequence of direct energy transfer to the lattice governed by both spin-orbit coupling and exchange interaction in all magnetic materials [14,15]. The latter mechanism is a non-Gilbert-type relaxation, divided mainly into two categories [14,15]—(i) the magnetic inhomogeneity induced broadening: inhomogeneity in the internal static magnetic field, and the crystallographic axis orientation, and (ii) two-magnon scattering: the energy dissipates in the spin subsystem by virtue of magnon scattering with nonzero wave vector, $k \neq 0$, where the uniform resonance mode couples with the degenerate spin waves. The angular variation of ferromagnetic resonance field (H_r) provides information about the presence of different magnetic anisotropies in magnetic crystals [4,6]. Most attention has been paid toward the angular dependence of H_r [4,6], whereas the angular variation of the ΔH is sparsely investigated. The studies involving angular dependence of ΔH may help to probe different contributions to the precessional damping.

The radio frequency magnetization dynamics on the YIG-GdIG heterostructure still remains unexplored and needs a detailed ferromagnetic resonance (FMR) study. In this paper, we investigate the effect of the growth-induced interfacial GdIG layer on the magnetization dynamics of antiferromagnetically (AFM) exchange coupled YIG film. An enhanced value of $\alpha \sim 1.2 \times 10^{-3}$ is realized for a 200 nm thick YIG film, which is more than an order of magnitude higher than what is usually seen in YIG films [1,2,16,17]. We observe an unusual behavior in the out-of-plane angular variation of ΔH where spin inhomogeneity at the interface plays a significant role in defining the ΔH broadening and enhanced α. In-plane angular variation showing a unidirectional feature demands the incorporation of an exchange anisotropy to the free-energy density, indicating the presence of an AFM exchange coupling at the YIG-GdIG interface [12], and may give rise to a large $\Delta 4\pi M_{\rm eff}$. This extrinsic $\Delta 4\pi M_{\rm eff}$ contribution due to spin inhomogeneity at the interface adds up to the inherent Gilbert contribution, which may lead to a significant enhancement in precessional damping. We performed a control experiment on YIG/GGG(111) specimens of thicknesses 200, 100, and 32 nm. Our study unveils that the formation of an interfacial GdIG layer AFM exchange coupled to YIG can have dramatic effects on its magnetization dynamics.

*kumar.ravinderraj@gmail.com

†zakir@iitk.ac.in

 ©2022 American Physical Society

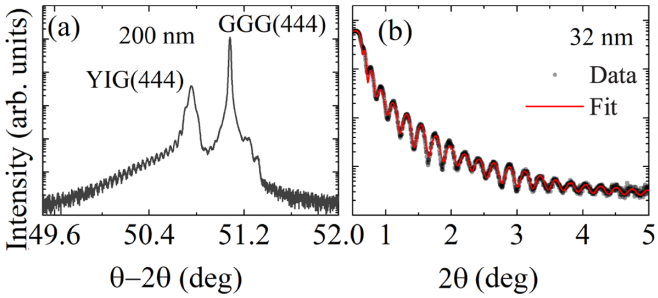

FIG. 1. Structural characterization of YIG films using x-ray diffraction technique. (a) Representative x-ray diffraction pattern of a 200 nm thick film showing trails of Laue oscillation along with a broad humplike feature beneath film-substrate (444) reflection. (b) X-ray reflectivity pattern of a 32 nm thick YIG film to calculate the film thickness. The fitting gives ∼5 nm thin interfacial GdIG layer at the YIG-GGG interface.

II. SAMPLE AND MEASUREMENT SETUPS

We deposit epitaxial YIG films on GGG(111) substrate by employing a KrF excimer laser (Lambda Physik COMPex Pro, $\lambda = 248$ nm) of 20 ns pulse width. A solid state synthesized $Y_3Fe_5O_{12}$ target is ablated using an areal energy of 2.12 J cm^{-2} with a repetition frequency of 10 Hz. The GGG(111) substrate is placed 50 mm away from the target. Using the above growth parameters, a 200 nm thick film was deposited at 800 °C temperature and post-deposition annealed at the same temperature for 60 minutes [3]. The structural properties are characterized using a Panalytical X'pert Pro x-ray diffraction setup. We also deposit 32 and 100 nm thick YIG films for thickness-dependent study. FMR measurements are performed using a Bruker EMX EPR spectrometer and a broadband coplanar waveguide setup. The former technique uses a cavity mode frequency $f \approx 9.60$ GHz, and enables us to perform FMR spectra for various θ_H and ϕ_H angular variations. The latter technique enables us to measure frequency-dependent ferromagnetic resonance (FMR) spectra. We define the configurations **H** parallel ($\theta_H = 90°$) and perpendicular ($\theta_H = 0°$) to the film plane for rf frequency and angular dependent measurements. The resultant spectra are obtained as the derivative of microwave absorption with respect to the applied field **H**.

III. RESULTS AND DISCUSSION

A. X-ray diffraction

Figure 1 shows representative x-ray diffraction (XRD) and x-ray reflectivity (XRR) measurements performed on epitaxially grown YIG thin films. The θ-2θ XRD pattern of a 200 nm thick film shown in Fig. 1(a) exhibits trails of Laue oscillations, indicating epitaxial growth. This sample was used in a previous study for preliminary structural and static magnetization characterizations [3]. If we look at the plot [Fig. 1(a)], we can observe (444) reflections from GGG substrate and YIG film. Also, there is a broad humplike discernible feature present beneath film-substrate (444) reflection. The broad humplike feature appearing in data represents the GdIG interfacial layer [13], which was not discussed in the earlier work. We performed XRR to measure the film thickness as shown in Fig. 1(b) for a 32 nm thick YIG film. We fitted the experimental data by considering an extremely thin GdIG layer at the film-substrate interface, and the realized GdIG thickness is ∼5 nm. The experimental data and fitting are represented by gray dots and the red line, respectively.

B. Broadband FMR

Figure 2(a) shows typical broadband FMR spectra in a frequency f range of 1.5 to 13 GHz for 200 nm thick YIG film at temperature $T = 300$ K and $\theta_H = 90°$. The mode appearing at a lower field value is the main mode, whereas the one at a higher field value represents the surface mode. We discuss all these features in detail in Sec. III C. We determine H_r and ΔH from the first derivative of the absorption spectra. Figure 2(b) shows the rf frequency dependence of H_r at $\theta_H = 90°$ and 0°. We use the Kittel equation for fitting the frequency vs H_r data from the resonance condition expressed as [10] $f = \gamma[H_r(H_r + 4\pi M_{\text{eff}})]^{1/2}/(2\pi)$ for $\theta_H = 90°$ and $f = \gamma(H_r - 4\pi M_{\text{eff}})/(2\pi)$ for $\theta_H = 0°$, where $\gamma = g\mu_B/\hbar$ is the gyromagnetic ratio, and $4\pi M_{\text{eff}} = 4\pi M_S - H_{\text{ani}}$ is the effective magnetization consisting of $4\pi M_S$ saturation magnetization [calculated using $M(H)$] and H_{ani} anisotropy field parametrizing cubic and out-of-plane uniaxial anisotropies. The fitting gives $4\pi M_{\text{eff}} \approx 2000$ Oe, which is used to calculate the $H_{\text{ani}} \approx -370$ Oe. Similarly, the $4\pi M_{\text{eff}}$ values for 100 and 32 nm films are 2088 and 2211 Oe, respectively.

Figure 2(c) shows the frequency dependence of ΔH at $\theta_H = 90°$. The intrinsic and extrinsic damping contributions are responsible for a finite width of the FMR signal. The intrinsic damping ΔH_{int} arises due to the Gilbert damping of the precessing moments, whereas the extrinsic damping ΔH_{ext} exists due to different non-Gilbert-type relaxations such as inhomogeneity due to the distribution of magnetic anisotropy ΔH_{inhom}, or two-magnon scattering (TMS) ΔH_{TMS}. The intrinsic Gilbert damping coefficient (α) can be determined using the Landau-Lifshitz-Gilbert equation expressed as [10] $\Delta H = \Delta H_{\text{int}} + \Delta H_{\text{inhom}} = (4\pi\alpha/\sqrt{3}\gamma)f + \Delta H_{\text{inhom}}$. Considering the above equation, where ΔH obeys linear f dependence, the slope determines the value of α, and ΔH_{inhom} corresponds to the intercept on the vertical axis. We observe a very weak nonlinearity in the f dependence of ΔH, which is believed to be due to the contribution of TMS to the linewidth, ΔH_{TMS}. The nonlinear f dependence of ΔH in Fig. 2(c) can be described in terms of TMS, assuming $\Delta H = \Delta H_{\text{int}} + \Delta H_{\text{inhom}} + \Delta H_{\text{TMS}}$. We put a factor of $1/\sqrt{3}$ to ΔH due to the peak-to-peak linewidth value extraction [14]. The TMS induces nonlinear slope at low frequencies, whereas a saturation is expected at high frequencies. TMS is induced by scattering centers and surface defects in the sample. The defects with size comparable to the wavelength of spin waves are supposed to act as scattering centers. The TMS term at $\theta_H = 90°$ can be expressed as [18]

$$\Delta H_{\text{TMS}}(\omega) = \Gamma \sin^{-1}\sqrt{\frac{\sqrt{\omega^2 + (\omega_0/2)^2} - \omega_0/2}{\sqrt{\omega^2 + (\omega_0/2)^2} + \omega_0/2}}, \quad (1)$$

with $\omega = 2\pi f$ and $\omega_0 = \gamma 4\pi M_{\text{eff}}$. The prefactor Γ defines the strength of TMS. The extracted values are as follows:

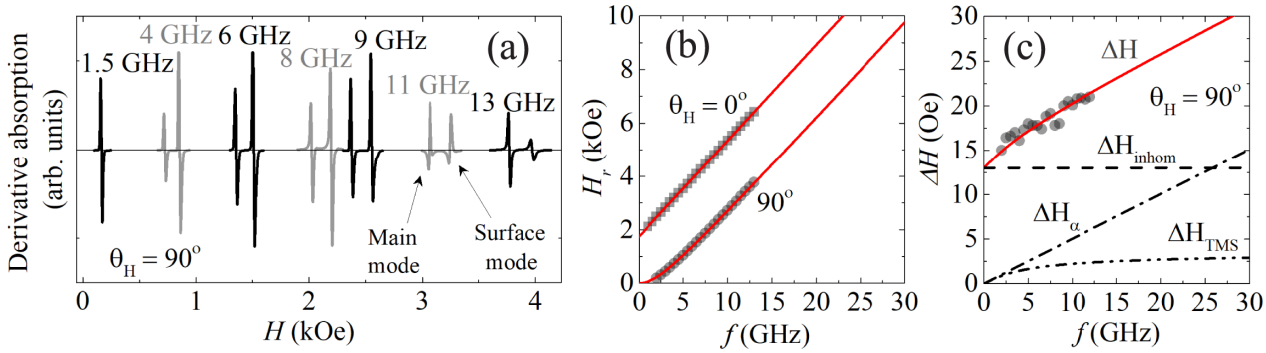

FIG. 2. Room temperature frequency dependent FMR measurements on 200 nm thick film. (a) Representative FMR derivative spectra for different frequencies at $\theta_H = 90°$. (b) Resonance field vs frequency data for $\theta_H = 90°$ and $\theta_H = 0°$ are represented using circle and square data points in gray color, respectively. The fittings to both the data are shown using red lines. (c) Linewidth vs frequency data at $\theta_H = 90°$. The filled gray circles represent experimental data, whereas the solid red line represents ΔH fitting. Inhomogeneous (ΔH_{inhom}), Gilbert (ΔH_α), and two-magnon scattering (ΔH_{TMS}) contributions to ΔH are shown using dashed, dash-dotted, and dash-dot-dotted lines, respectively.

$\alpha = 1.2 \times 10^{-3}$, $\Delta H_0 = 13$ Oe, and $\Gamma = 2.5$ Oe. The Gilbert damping for even very thin YIG film is extremely low, $\sim 6 \times 10^{-5}$, whereas the value we achieved is higher than that reported in the literature for YIG thin films [2,16,17]. Also, the value of Γ is insignificant, implying negligible contribution to the damping. Similarly, we extract these parameters for 100 nm ($\alpha = 3.7 \times 10^{-3}$ and $\Delta H_0 = 12$ Oe) and 32 nm ($\alpha = 8.9 \times 10^{-3}$ and $\Delta H_0 = 19$ Oe) thick YIG/GGG(111) specimens.

C. Cavity FMR

Figure 3(a) shows typical $T = 300$ K cavity-FMR ($f \approx 9.6$ GHz) spectra for 200 nm thick YIG film performed at different θ_H. The FMR spectra exhibit some universal features: (i) a spin-wave resonance (SWR) spectrum for $\theta_H = 0°$, (ii) rotating the **H** away from the $\theta_H = 0°$; the SWR modes successively start diminishing, and at certain critical angle θ_c [which falls in a range of 30°–35°; shaded region in Fig. 3(b)], all the modes vanish except a single mode (uniform FMR mode). With further rotation of **H** for $\theta_H > \theta_c$, the SWR modes start reemerging. We observe that the SWR mode appearing at the higher-field side for $\theta_H > \theta_c$ represents an exchange-dominated nonpropagating surface mode [19–21]. The above discussed complexity in H_r vs θ_H behavior has already been realized in some material systems [21], including a μm-thick YIG film [20]. The localized mode or surface spin-wave mode appears for **H** $\parallel$ but not $\perp$ to the film plane [19–21]. We assign the SWR modes for the sequence $n = 1, 2, 3, \ldots$, as it provides the best correspondence to $H_{ex} \propto n^2$, where $H_{ex} = H_r(n) - H_r(0)$ defines exchange field [22]. The exchange stiffness can be obtained by considering the modified Schreiber and Frait classical approach using the mode number n^2 dependence of H_{ex} [inset Fig. 3(b)] [22]. For a fixed frequency, the exchange field H_{ex} of thickness modes is determined by subtracting the highest-field resonance mode ($n = 1$) from the higher modes ($n \neq 1$). In the modified Schreiber and Frait equation, the H_{ex} shows direct dependency on the exchange stiffness D: $\mu_0 H_{ex} = D\frac{\pi^2}{d^2}n^2$ (where d is the film thickness). The linear fit of data shown in the inset of Fig. 3(b) gives $D = 3.15 \times 10^{-17}$ T m^2. The exchange stiffness constant A can be determined using the relation $A = D M_S/2$. The

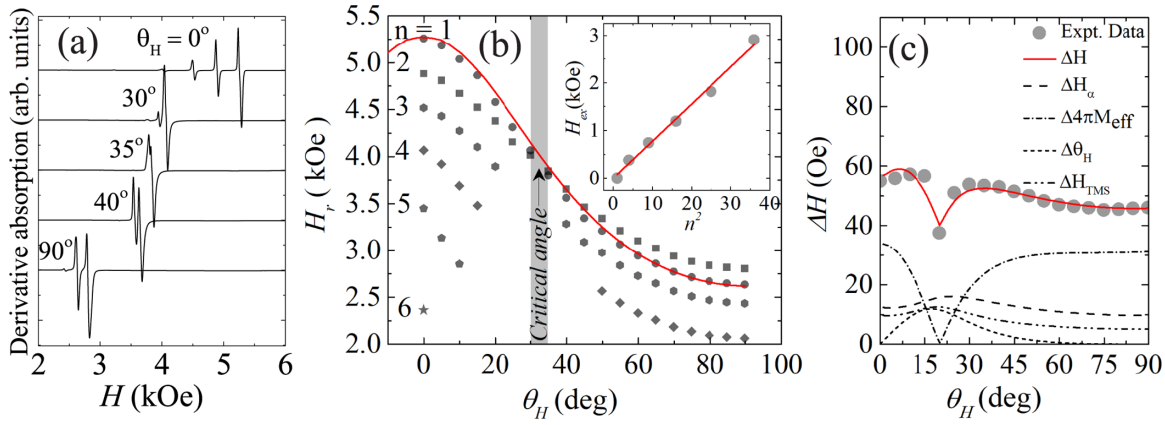

FIG. 3. Room temperature out-of-plane angular θ_H dependence of FMR on 200 nm thick YIG film. (a) Derivative FMR spectra shown for different θ_H performed at ≈9.6 GHz. (b) θ_H variation of uniform mode and SWR modes of H_r. Inset: Exchange field (H_{ex}) vs mode number square (n^2). (c) θ_H variation of ΔH, where the experimental and simulated data are represented by filled gray circles and red line, respectively. The different contributions ΔH_α, $\Delta 4\pi M_{\text{eff}}$, $\Delta\theta_H$, and ΔH_{TMS} are represented by dashed, dash-dotted, small-dashed, and dash-dot-dotted lines, respectively.

calculated value is $A = 2.05$ pJ m^{-1}, which is comparable to the value calculated for YIG, $A = 3.7$ pJ m^{-1} [22].

YIG thin films with in-plane easy magnetization exhibit extrinsic uniaxial magnetic and intrinsic magnetocrystalline cubic anisotropies [23]. The total free energy density for YIG(111) is given by [23,24]

$$\begin{aligned} F = & -HM_S\begin{bmatrix}\sin\theta_H\sin\theta_M\cos(\phi_H-\phi_M)\\ +\cos\theta_H\cos\theta_M\end{bmatrix}\\ & +2\pi M_S^2\cos^2\theta_M - K_u\cos^2\theta_M\\ & +\frac{K_1}{12}\begin{pmatrix}7\sin^4\theta_M - 8\sin^2\theta_M + 4-\\ 4\sqrt{2}\sin^3\theta_M\cos\theta_M\cos 3\phi_M\end{pmatrix}\\ & +\frac{K_2}{108}\begin{pmatrix}-24\sin^6\theta_M + 45\sin^4\theta_M - 24\sin^2\theta_M + 4\\ -2\sqrt{2}\sin^3\theta_M\cos\theta_M\left(5\sin^2\theta_M - 2\right)\cos 3\phi_M\\ +\sin^6\theta_M\cos 6\phi_M\end{pmatrix}. \end{aligned} \tag{2}$$

Equation (2) consists of the following different energy terms: the first term is the Zeeman energy, the second term is the demagnetization energy, the third term is the out-of-plane uniaxial magnetocrystalline anisotropy energy K_u, and the last two terms are the first and second order cubic magnetocrystalline anisotropy energies (K_1 and K_2), respectively. The total free energy density equation is minimized by taking partial derivatives with respect to θ_M and ϕ_M to obtain the equilibrium orientation of the magnetization vector $\mathbf{M}(\mathbf{H})$, i.e., $\partial F/\partial\theta_M = \partial F/\partial\phi_M = 0$. The resonance frequency of uniform precession at equilibrium condition is expressed as [23,25,26]

$$\omega_{\text{res}} = \frac{\gamma}{M_S\sin\theta_M}\left[\frac{\partial^2 F}{\partial\theta_M^2}\frac{\partial^2 F}{\partial\phi_M^2} - \left(\frac{\partial^2 F}{\partial\theta_M\partial\phi_M}\right)^2\right]^{1/2}. \tag{3}$$

Mathematica is used to numerically solve the resonance condition described by Eq. (3) for the energy density given by Eq. (2). The solution for a fixed frequency is used to fit the angle-dependent resonance data (H_r vs θ_H) shown in Fig. 3(b). The main mode data simulation is shown using a black line. The parameters obtained from the simulation are $K_u = -1.45\times10^4$ ergs cm^{-3}, $K_1 = -1.50\times10^3$ ergs cm^{-3}, and $K_2 = 0.13\times10^3$ ergs cm^{-3}. The calculated uniaxial anisotropy field value is $H_u \sim -223$ Oe. These parameters are comparable to the reported values for YIG films [3,23,27,28].

The ΔH manifests the spin dynamics and related relaxation mechanisms in a magnetic system. The intrinsic contribution to ΔH arises due to the Gilbert term $\Delta H_{\text{int}} \approx \Delta H_\alpha$, whereas, the extrinsic contribution ΔH_{ext} consists of line broadening due to ΔH_{inhom} and ΔH_{TMS}. The terms representing the precessional damping due to intrinsic and extrinsic contributions can be expressed in different phenomenological forms. Figure 3(c) shows ΔH as a function of θ_H. The θ_H variation of ΔH shows distinct signatures due to different origins of magnetic damping. We consider both ΔH_{int} and ΔH_{ext} magnetic damping contributions to the broadening of ΔH, $\Delta H = 1/\sqrt{3}\Delta H_\alpha + 1/\sqrt{3}\Delta H_{\text{inhom}} + 1/\sqrt{3}\Delta H_{\text{TMS}}$. The first term can be expressed as [14]

$$\Delta H_\alpha = \frac{\alpha}{M_S}\left[\frac{\partial^2 F}{\partial\theta_M^2} + \frac{1}{\sin^2\theta_M}\frac{\partial^2 F}{\partial\phi_M^2}\right]\left|\frac{\partial(\frac{2\pi f}{\gamma})}{\partial H_r}\right|^{-1}. \tag{4}$$

The second term ΔH_{inhom} has the form [14]

$$\Delta H_{\text{inhom}} = \left|\frac{dH_r}{d4\pi M_{\text{eff}}}\right|\Delta 4\pi M_{\text{eff}} + \left|\frac{dH_r}{d\theta_H}\right|\Delta\theta_H, \tag{5}$$

where the dispersion of magnitude and direction of the $4\pi M_{\text{eff}}$ are represented by $\Delta 4\pi M_{\text{eff}}$ and $\Delta\theta_H$, respectively. The ΔH_{inhom} contribution arises due to a small spread of the sample parameters such as thickness, internal fields, or orientation of crystallites within the thin film. The third term ΔH_{TMS} can be written as [29]

$$\Delta H_{\text{TMS}} = \sum_{i=1}\frac{\Gamma_i^{\text{out}} f_i(\phi_H)}{\mu_0\gamma\Phi}\sin^{-1}\sqrt{\frac{\sqrt{\omega^2+(\omega_0/2)^2}-\omega_0/2}{\sqrt{\omega^2+(\omega_0/2)^2}+\omega_0/2}},$$
$$\Gamma_i^{\text{out}} = \Gamma_i^0\Phi A(\theta-\pi/4)\frac{dH_r(\theta_H)}{d\omega(\theta_H)}\Big/\frac{dH_r(\theta_H=0)}{d\omega(\theta_H=0)}. \tag{6}$$

The prefactor Γ_i^{out} defines the TMS strength and has a θ_H dependency in this case. The type and size of the defects responsible for TMS are difficult to characterize which makes it nontrivial to express the exact form of Γ_i^{out}. However, it may have a simplified expression given in Eq. (6), where Γ_i^0 is a constant, $A(\theta-\pi/4)$ is a step function which makes sure that the TMS is deactivated for $\theta_H > \pi/4$, and $dH_r(\theta_H)/d\omega(\theta_H)$ is a normalization factor responsible for the θ_H dependence of the Γ_i^{out}. In Fig. 3(c) the filled gray circles and red solid line represent the experimental and simulated ΔH vs θ_H data, respectively. We also plot contributions of different terms such as ΔH_α (dashed line), $\Delta 4\pi M_{\text{eff}}$ (dash-dotted line), $\Delta\theta_H$ (small-dashed line), and ΔH_{TMS} (dash-dot-dotted line). The fitting provides the following extracted parameters, g factor $\sim$2.010, $\alpha = 1.3\times10^{-3}$, $\Delta 4\pi M_{\text{eff}} = 58$ Oe, $\Delta\theta_H = 0.29^\circ$, and $\Gamma_i^0 = 1.3$ Oe. The precessional damping calculated from the ΔH vs θ_H corroborates with the value extracted from the frequency dependence of ΔH data [shown in Fig. 2(c)], $\alpha = 1.2\times10^{-3}$. The ΔH broadening and the overwhelmingly enhanced precessional damping are the direct consequence of contributions from intrinsic and extrinsic damping. Usually, the Gilbert term and the inhomogeneity due to sample quality contribute to the broadening of ΔH and enhanced α in YIG thin films. From our analysis of ΔH vs θ_H data, it is clear that damping enhancement in YIG is arising from the extrinsic magnetic inhomogeneity.

The role of an interface in YIG coupled with metals or insulators leading to the increments in ΔH and α has been vastly explored. Wang *et al.* [9] studied a variety of insulating spacers between YIG and Pt to probe the effect on spin pumping efficiency. Their results suggest the generation of magnetic excitations in the adjacent insulating layers due to the precessing magnetization in YIG at resonance. This happens due to either fluctuating correlated moments or antiferromagnetic ordering, via interfacial exchange coupling, leading to ΔH broadening and enhanced precessional damping of the YIG [9]. The impurity relaxation mechanism is also responsible for ΔH broadening and enhanced magnetic damping in YIG, but is prominent only at low temperatures [18]. Strong enhancement in magnetic damping of YIG capped with Pt has been observed by Sun *et al.* [8]. They suggest ferromagnetic ordering in an atomically thin Pt layer due to proximity with YIG at the YIG-Pt interface, which

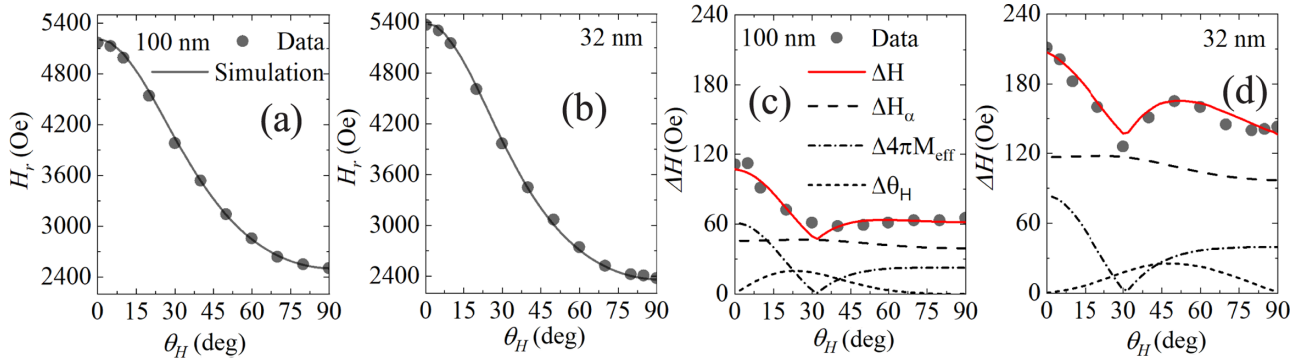

FIG. 4. Room temperature out-of-plane angular θ_H dependence of FMR performed at ≈9.6 GHz. The θ_H variation of H_r for (a) 100 and (b) 32 nm thick YIG/GGG(111) specimens. The experimental and simulated data are represented by filled gray circles and solid black line, respectively. The θ_H variation of ΔH for (c) 100 nm and (d) 32 nm YIG/GGG(111) specimens. The experimental and simulated data are represented by filled gray circles and red lines, respectively. The different contributions ΔH_α, $\Delta 4\pi M_{\text{eff}}$, and $\Delta\theta_H$ are represented by dashed, dash-dotted, and small-dashed lines, respectively.

dynamically exchange couples to the spins in YIG [8]. In recent years, some research groups have reported the presence of a thin interfacial layer at the YIG-GGG interface [11–13]. The 200 nm film we used in this study is of high quality with trails of sharp Laue oscillations [see Fig. 1(a)]. Thus it is quite clear that the observed ΔH broadening and enhanced α is not a consequence of sample inhomogeneity. The formation of an interfacial GdIG layer at the YIG-GGG interface, which exchange couples with the YIG film, may lead to ΔH broadening and increased α. Considering the above experimental evidence leading to ΔH broadening and enhanced Gilbert damping due to coupling with metals and insulators [8,9], it is safe to assume that the interfacial GdIG layer at the interface AFM exchange couples with the YIG [11–13], and is responsible for enhanced ΔH and α.

To further substantiate that the enhancement in Gilbert damping and the linewidth broadening is a consequence of AFM exchange coupling at the YIG-GdIG interface, we performed angular FMR measurement on two relatively thinner YIG films of nominal thicknesses 32 and 100 nm. Figures 4(a) and 4(b) show H_r vs θ_H variation of 100 and 32 nm YIG/GGG(111) specimens, respectively. The simulation was performed using Eqs. (2) and (3), and is shown by the black line. The extracted parameters for 100 nm thick YIG film are $K_u = -2.13 \times 10^4$ ergs cm^{-3}, $K_1 = -2.30 \times 10^3$ ergs cm^{-3}, $K_2 = 1.42 \times 10^2$ ergs cm^{-3}, and $H_{\text{ani}} = -531$ Oe. Similarly, these parameters for 32 nm thick film are $K_u = -4.19 \times 10^4$ ergs cm^{-3}, $K_1 = -2.50 \times 10^3$ ergs cm^{-3}, $K_2 = 1.61 \times 10^2$ ergs cm^{-3}, and $H_{\text{ani}} = -804$ Oe. Figures 4(c) and 4(d) show ΔH vs θ_H variation for 100 and 32 nm YIG/GGG(111) specimens, respectively. The extracted parameters for the 100 nm YIG/GGG(111) specimen are g factor ∼2.022, $\alpha = 4 \times 10^{-3}$, $\Delta 4\pi M_{\text{eff}} = 65$ Oe, and $\Delta\theta_H = 0.8°$. Similarly, for the 32 nm YIG/GGG(111) specimen, they are g factor ∼2.058, $\alpha = 9 \times 10^{-3}$, $\Delta 4\pi M_{\text{eff}} = 90$ Oe, and $\Delta\theta_H = 2.6°$. It is noteworthy that the Gilbert damping, along with other parameters such as $\Delta 4\pi M_{\text{eff}}$ and $\Delta\theta_H$, is enhanced as we decrease the film thickness. The increment in $\Delta 4\pi M_{\text{eff}}$ and $\Delta\theta_H$ signifies the dominance of AFM exchange coupling at the YIG-GdIG interface as the total magnetic volume of YIG is reduced [12,30]. This implies that an AFM exchange coupling between the growth-induced GdIG-interfacial layer and top-YIG layer plays a crucial role in the magnetization dynamics of the YIG thin film.

Figure 5 shows in-plane ϕ_H angular variation of H_r for the YIG/GGG(111) specimens. We simulate the in-plane H_r vs ϕ_H angular variation using the free energy densities provided in Ref. [31] and an additional term, $-K_{EA} \sin\theta_M \cos\phi_M$, representing the exchange anisotropy (K_{EA}). A unidirectional anisotropy trend is visible in Fig. 5, suggesting an AFM exchange coupling between the interface and YIG. The values of exchange anisotropy for YIG/GGG(111) specimens are as follows—(i) 200 nm: $K_{EA} = -0.9 \times 10^3$ ergs cm^{-3}, (ii) 100 nm: $K_{EA} = -1.2 \times 10^3$ ergs cm^{-3}, and (iii) 32 nm: $K_{EA} = -1.1 \times 10^3$ ergs cm^{-3}. Figures 5(a) and 5(b) show a prominent feature of unidirectional anisotropy in 200 and 100 nm thick YIG/GGG(111) specimens, respectively, whereas the unidirectional feature is suppressed in the 32 nm thick YIG/GGG(111) specimen [shown in Fig. 5(c)] due to the presence of a large in-plane uniaxial anisotropy. The lattice strain increases as the film thickness decreases, which leads to large uniaxial anisotropy in thin films. It is noteworthy that the AFM exchange coupling at the YIG-GdIG interface leading to a unidirectional feature due to exchange anisotropy is almost the same for all the YIG/GGG(111) specimens. It has been shown that the large inhomogeneous $4\pi M_{\text{eff}}$ is a direct consequence of the AFM exchange coupling at the interface of LSMO and a growth-induced interfacial layer [30]. The YIG thin film system due to the presence of a hard ferrimagnetic GdIG interfacial layer possesses AFM exchange coupling [11–13]. The literature suggests that a Bloch domain-wall-like spiral moments arrangement may take place due to the AFM exchange coupling across the interfacial GdIG and top bulk YIG layer [11–13,30]. An exchange springlike characteristic is found in YIG film due to the spiral arrangement of the magnetic moments [11–13]. The FMR measurement and the extracted value of $\Delta 4\pi M_{\text{eff}}$ reflect inhomogeneous distribution of $4\pi M_{\text{eff}}$ in the YIG-GdIG bilayer system. The argument of the Bloch domain-wall-like spiral arrangement of moments is conceivable, as this arrangement between the adjacent layers lowers the exchange interaction energy [30]. It is evident that the interfacial layer exchange couples with

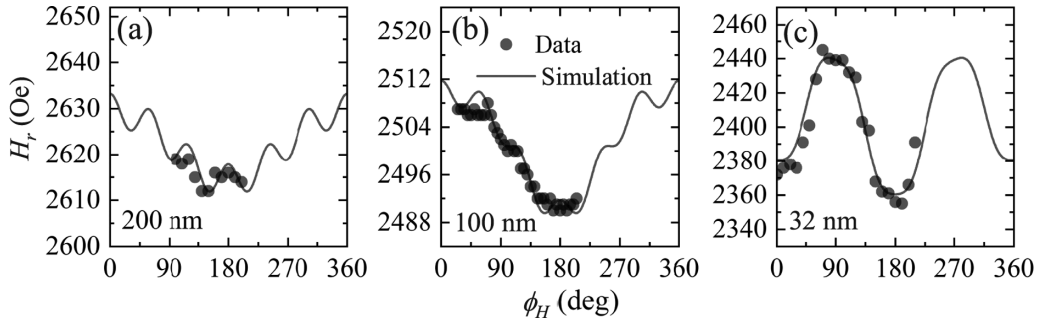

FIG. 5. Room temperature in-plane angular ϕ_H variation of H_r for (a) 200 nm, (b) 100 nm, and (c) 32 nm thick YIG/GGG(111) specimen. The experimental data are represented by filled gray circles, whereas the simulated data for total and exchange (unidirectional) anisotropy are represented by solid black line.

the top YIG film and leads to a unidirectional anisotropy. We observe that the interfacial exchange coupling may cause ΔH broadening and enhanced damping due to spin inhomogeneity at the YIG-GdIG interface, even in a 200 nm thick YIG film.

IV. CONCLUSIONS

The effects of spin inhomogeneity at the YIG and growth-induced GdIG interface on the magnetization dynamics of YIG/GGG(111) specimens is studied extensively using the ferromagnetic resonance technique. The Gilbert damping is more than an order of magnitude larger ($\sim 1.2 \times 10^{-3}$) than usually reported in YIG thin films. The out-of-plane angular dependence of ΔH shows an unusual behavior which can only be justified after considering an extrinsic mechanism in combination with the Gilbert contribution. The extracted parameters for a 200 nm thick YIG film from the ΔH vs θ_H simulation are (i) $\alpha = 1.3 \times 10^{-3}$ from the Gilbert term; (ii) $\Delta 4\pi M_{\text{eff}} = 58$ Oe and $\Delta\theta_H = 0.29^\circ$ from the inhomogeneity in effective magnetization and anisotropy axes, respectively; (iii) $\Gamma_i^0 = 1.3$ Oe from TMS. The TMS strength Γ is not so appreciable, indicating a high-quality thin film with insignificant defect sites. The AFM exchange coupling between YIG and the interfacial GdIG layer causes spin inhomogeneity at the interface, leading to a large $\Delta 4\pi M_{\text{eff}}$. The presence of large $\Delta 4\pi M_{\text{eff}}$ impels the quick dragging of the precessional motion toward equilibrium. A thickness-dependent study suggests that the inhomogeneity in the $\Delta 4\pi M_{\text{eff}}$ increases with lowering the YIG film thickness. A unidirectional behavior is observed in the in-plane angular variation of resonance field due to the presence of an exchange anisotropy, $K_{EA} \sim 10^3$ ergs cm^{-3}. This further reinforces the spin inhomogeneity at the YIG-GdIG interface due to the AFM exchange coupling.

ACKNOWLEDGMENTS

We gratefully acknowledge the research support from IIT Kanpur and SERB, Government of India (Grant No. CRG/2018/000220). R.K. and D.S. acknowledge the financial support from the Max Planck partner group. Z.H. acknowledges financial support from the Polish National Agency for Academic Exchange under the Ulam Fellowship. The authors thank Veena Singh for her help with the angular-dependent FMR measurements.

[1] M. Sparks, *Ferromagnetic-Relaxation Theory*, Advanced Physics Monograph Series (McGraw-Hill, 1964).
[2] C. Hauser, T. Richter, N. Homonnay, C. Eisenschmidt, M. Qaid, H. Deniz, D. Hesse, M. Sawicki, S. G. Ebbinghaus, and G. Schmidt, Sci. Rep. **6**, 20827 (2016).
[3] R. Kumar, Z. Hossain, and R. C. Budhani, J. Appl. Phys. **121**, 113901 (2017).
[4] H. Wang, C. Du, P. C. Hammel, and F. Yang, Phys. Rev. B **89**, 134404 (2014).
[5] L. E. Helseth, R. W. Hansen, E. I. Il'yashenko, M. Baziljevich, and T. H. Johansen, Phys. Rev. B **64**, 174406 (2001).
[6] R. Kumar, B. Samantaray, and Z. Hossain, J. Phys.: Condens. Matter **31**, 435802 (2019).
[7] M. C. Onbasli, L. Beran, M. Zahradnĺk, M. Kučera, R. Antoš, J. Mistrĺk, G. F. Dionne, M. Veis, and C. A. Ross, Sci. Rep. **6**, 23640 (2016).
[8] Y. Sun, H. Chang, M. Kabatek, Y.-Y. Song, Z. Wang, M. Jantz, W. Schneider, M. Wu, E. Montoya, B. Kardasz, B. Heinrich, S. G. E. te Velthuis, H. Schultheiss, and A. Hoffmann, Phys. Rev. Lett. **111**, 106601 (2013).
[9] H. Wang, C. Du, P. C. Hammel, and F. Yang, Phys. Rev. B **91**, 220410(R) (2015).
[10] H. Chang, P. A. Praveen Janantha, J. Ding, T. Liu, K. Cline, J. N. Gelfand, W. Li, M. C. Marconi, and M. Wu, Sci. Adv. **3**, e1601614 (2017).
[11] E. L. Jakubisova, S. Visnovsky, H. Chang, and M. Wu, Appl. Phys. Lett. **108**, 082403 (2016).
[12] J. M. Gomez-Perez, S. Vélez, L. McKenzie-Sell, M. Amado, J. Herrero-Martín, J. López-López, S. Blanco-Canosa, L. E. Hueso, A. Chuvilin, J. W. A. Robinson, and F. Casanova, Phys. Rev. Appl. **10**, 044046 (2018).
[13] R. Kumar, S. N. Sarangi, D. Samal, and Z. Hossain, Phys. Rev. B **103**, 064421 (2021).
[14] S. J. Yuan, L. Sun, H. Sang, J. Du, and S. M. Zhou, Phys. Rev. B **68**, 134443 (2003).
[15] K. Zakeri, J. Lindner, I. Barsukov, R. Meckenstock, M. Farle, U. von Hörsten, H. Wende, W. Keune, J. Rocker, S. S. Kalarickal, K. Lenz, W. Kuch, K. Baberschke, and Z. Frait, Phys. Rev. B **76**, 104416 (2007).

[16] C. Hahn, G. de Loubens, O. Klein, M. Viret, V. V. Naletov, and J. Ben Youssef, Phys. Rev. B **87**, 174417 (2013).
[17] M. B. Jungfleisch, A. V. Chumak, A. Kehlberger, V. Lauer, D. H. Kim, M. C. Onbasli, C. A. Ross, M. Kläui, and B. Hillebrands, Phys. Rev. B **91**, 134407 (2015).
[18] C. L. Jermain, S. V. Aradhya, N. D. Reynolds, R. A. Buhrman, J. T. Brangham, M. R. Page, P. C. Hammel, F. Y. Yang, and D. C. Ralph, Phys. Rev. B **95**, 174411 (2017).
[19] C. Vittoria and J. H. Schelleng, Phys. Rev. B **16**, 4020 (1977).
[20] J. T. Yu, R. A. Turk, and P. E. Wigen, Phys. Rev. B **11**, 420 (1975).
[21] X. Liu, Y. Y. Zhou, and J. K. Furdyna, Phys. Rev. B **75**, 195220 (2007).
[22] S. Klingler, A. V. Chumak, T. Mewes, B. Khodadadi, C. Mewes, C. Dubs, O. Surzhenko, B. Hillebrands, and A. Conca, J. Phys. D **48**, 015001 (2015).
[23] S. Lee, S. Grudichak, J. Sklenar, C. C. Tsai, M. Jang, Q. Yang, H. Zhang, and J. B. Ketterson, J. Appl. Phys. **120**, 033905 (2016).
[24] L. D. Landau and E. M. Lifshitz, *Electrodynamics of Continuous Media*, 2nd ed. (Pergamon Press, Oxford, 1984).
[25] H. Suhl, Phys. Rev. **97**, 555 (1955).
[26] J. Smit and H. G. Beljers, Philips Res. Rep. **10**, 113 (1955).
[27] S. A. Manuilov, S. I. Khartsev, and A. M. Grishin, J. Appl. Phys. **106**, 123917 (2009).
[28] S. A. Manuilov and A. M. Grishin, J. Appl. Phys. **108**, 013902 (2010).
[29] H. Kurebayashi, T. D. Skinner, K. Khazen, K. Olejník, D. Fang, C. Ciccarelli, R. P. Campion, B. L. Gallagher, L. Fleet, A. Hirohata, and A. J. Ferguson, Appl. Phys. Lett. **102**, 062415 (2013).
[30] P. Ghising, B. Samantaray, and Z. Hossain, Phys. Rev. B **101**, 024408 (2020).
[31] C. T. Wang, X. F. Liang, Y. Zhang, X. Liang, Y. P. Zhu, J. Qin, Y. Gao, B. Peng, N. X. Sun, and L. Bi, Phys. Rev. B **96**, 224403 (2017).